

Diversity of function and higher-order structure within HWE sensor histidine kinases

Igor Dikiy¹, Danielle Swingle^{1,2}, Kaitlyn Toy^{1,3}, Uthama R. Edupuganti^{1,2}, Giomar Rivera-Cancel⁴,
Kevin H. Gardner^{1,3,5*}

¹: Structural Biology Initiative, CUNY Advanced Science Research Center, New York, NY 10031

²: Ph.D. Program in Biochemistry, The Graduate Center – City University of New York, New York, NY
10016

³: Department of Chemistry and Biochemistry, City College of New York, New York, NY 10031

⁴: Department of Internal Medicine, UT Southwestern Medical Center, Dallas, TX 75390

⁵: Ph.D. Programs in Biochemistry, Biology, and Chemistry, The Graduate Center – City University of
New York, New York, NY 10016

*: direct correspondence to kgardner@gc.cuny.edu

ORCIDs:

Igor Dikiy: 0000-0002-8155-7788

Danielle Swingle: 0000-0003-3691-4560

Kaitlyn Toy: 0000-0003-2595-8779

Uthama R. Edupuganti: 0000-0003-0571-4101

Giomar Rivera-Cancel: 0000-0002-4909-4103

Kevin H. Gardner: 0000-0002-8671-2556

Keywords: histidine kinase, bacterial signal transduction, conformational change, structure-function, biophysics, environmental sensing, two-component system, HWE family, HisKA2 family

Running title: Diversity of function and structure in HWE family sensor HKs

29 **Abstract**

30 Integral to the protein structure/function paradigm, oligomeric state is typically conserved
31 along with function across evolution. However, notable exceptions such as the hemoglobins
32 show how evolution can alter oligomerization to enable new regulatory mechanisms. Here we
33 examine this linkage in histidine kinases (HKs), a large class of widely distributed prokaryotic
34 environmental sensors. While the majority of HKs are transmembrane homodimers,
35 members of the HWE/HisKA2 family can deviate from this architecture as exemplified by our
36 finding of a monomeric soluble HWE/HisKA2 HK (EL346, a photosensing Light-Oxygen-Voltage
37 (LOV)-HK). To further explore the diversity of oligomerization states and regulation within this
38 family, we biophysically and biochemically characterized multiple EL346 homologs and found a
39 range of HK oligomeric states and functions. Three LOV-HK homologs are primarily dimeric with
40 differing structural and functional responses to light, while two Per-ARNT-Sim (PAS)-HKs
41 interconvert between differentially active monomers and dimers, suggesting dimerization might
42 control enzymatic activity for these proteins. Finally, we examined putative interfaces in a
43 dimeric LOV-HK, finding that multiple regions contribute to dimerization. Our findings suggest
44 the potential for novel regulatory modes and oligomeric states beyond those traditionally defined
45 for this important family of environmental sensors.

46

47 **Introduction**

48 Sensor histidine kinases (HKs) are signal transduction receptors that are widespread in
49 prokaryotes, enabling these organisms to sense and respond to diverse environmental stimuli
50 (3, 4). HKs are typically found in two-component systems (TCS), which are most simply
51 composed of a sensor HK and a downstream response regulator (RR) co-located in the same
52 operon. The RR responds to a signal from the HK by acting as a phosphorylation-dependent
53 transcription regulator, with activation often triggering RR DNA binding and altering the
54 expression of nearby genes (5-8).

55 The prototypical sensor HK contains N-terminal sensor and C-terminal kinase domains,
56 the latter of which can be subdivided into a two-helix dimerization histidine phosphotransfer
57 (DHP) domain and a catalytic ATP-binding (CA) domain (9). The detection of a stimulus by the
58 sensor domain (or in some cases, elsewhere (8)) modulates the CA domain
59 autophosphorylation of a conserved His residue in the DHP domain; the phosphate group in this
60 phospho-His adduct is subsequently transferred to a conserved Asp in a downstream RR (5).

61 Most characterized sensor HKs are obligate homodimeric transmembrane receptors,
62 facilitating the transmission of signals across the membrane from periplasmic sensor domains to

63 cytoplasmic kinase domains via symmetry-breaking conformational changes (9-12). The
64 regulation of typical sensor HKs is largely believed to require a dimeric complex, both for the
65 structural changes between the “off” and “on” state as well as determining whether
66 autophosphorylation occurs between protomers (*in trans*) or within a protomer (*in cis*) (9, 13).
67 Dimerization is mediated via the DHp domains of two monomers, forming a four-helix bundle
68 and facilitating pivot-, piston-, or scissoring-type movements as part of the activation process (9,
69 14), echoing similar themes in integrins (15) and certain other transmembrane receptors. In
70 contrast, some sensors adopt different oligomeric states, such as the large multimeric
71 assemblies of chemotaxis HKs (16), hexameric KaiC circadian HKs (17) or the monomeric
72 photosensory EL346 HK (1, 18).

73 The traditional view of sensor HK structure has been built up from extensive structural
74 and biochemical studies (9) that have usually focused on HKs in only one of several subfamilies
75 of histidine kinases (the HisKA family within Pfam (19)). In contrast, the related HWE (His-Trp-
76 Glu)-HK and HisKA_2 families (referred to here as the HWE/HisKA2 family) of HKs have been
77 less studied from a structural perspective (14). Members of this group, which contain specific
78 sequence variations in the DHp and CA domains compared to members of the canonical HisKA
79 family, tend to signal to a more diverse set of output proteins which often lack DNA-binding
80 output domains (14). The HWE/HisKA2 family is also enriched in HKs lacking transmembrane
81 segments, likely localizing them to the cytosol. Notably, soluble sensor HKs are relieved of the
82 constraints of transmitting a signal across a lipid bilayer, which typically involves signal
83 transmission via motions of one protomer with respect to the other (9, 14). This raises several
84 questions: Are such soluble HKs able to adopt diverse oligomeric states, including non-dimeric
85 architectures? And could these varied architectures be equivalently varied in their regulation?
86 We view the relatively understudied HWE/HisKA2 family of HKs (14) as a suitable testbed for
87 these questions.

88 Our prior work on the HWE/HisKA2 family focused on three soluble HKs involved in the
89 general stress response of the marine alphaproteobacterium *Erythrobacter litoralis* HTCC2594
90 (EL346, EL362, and EL368) (1, 18, 20, 21). Each of these proteins senses blue light through a
91 light oxygen voltage (LOV) sensor domain (22, 23), a sub-class of the versatile Per-ARNT-Sim
92 (PAS) domains that are present in over 30% of HKs (4, 24). The response to blue light provides
93 a readily tractable way to explore the inactive and active states of histidine kinases, typically
94 corresponding to dark and light states of LOV-HKs (21, 25, 26). These states can be
95 conveniently distinguished spectrophotometrically: while the dark state spectra of LOV-HKs
96 exhibit a triplet peak at around 450 nm, characteristic of protein-bound flavin chromophores, the

97 light state spectrum has a broad, singlet absorption peak at 390 nm (27). This spectroscopic
98 change is due to the photochemically-triggered reduction of the flavin chromophore and
99 concomitant formation of a cysteine-C(4a) covalent adduct, a bond that is thermally reversible in
100 the dark on a timescale varying from seconds to hours among LOV domains (23).

101 While our prior studies indicate that EL368 is dimeric, EL346 is a soluble and functional
102 monomer (1, 20). The EL346 crystal structure reveals that it is held in a monomeric state by an
103 intramolecular association between its DHp-like domain and the LOV sensory domain, blocking
104 the face typically used for DHp domains to dimerize (1). Despite this deviation from current HK
105 signaling models, the monomeric EL346 undergoes light-induced increases in
106 autophosphorylation rate (1) as well as conformational changes involving the sensor, DHp, and
107 kinase domains (18). More broadly, the active monomer of EL346 suggests that soluble HKs
108 may not require dimerization as a key element in signal transduction, unlike conventional
109 transmembrane HKs.

110 To address this general issue in HK signaling, we set out to characterize the oligomeric
111 and functional states of several novel HWE/HisKA2 HKs. To do so, we used sequence similarity
112 searches to identify multiple soluble LOV- and PAS-HKs closely related to EL346, selecting five
113 proteins for in-depth analyses. We showed that three of these five are novel dimeric LOV-HKs,
114 each of which properly photocycles by UV-visible absorbance spectroscopy. Notably, these
115 LOV-HKs differed in the effect of light on their autophosphorylation activity, with a mix of dark-
116 and light-activated proteins among them. In addition, we also characterized two light-insensitive
117 PAS-HKs which equilibrate between monomeric and dimeric states with differing activities,
118 suggesting dimerization as a possible regulatory switch in this family of HKs. Finally, we
119 combined structural and sequence information to engineer a “monomerized dimer” by deleting
120 putative dimerization interfaces in a dimeric LOV-HK, finding that broadly distributed residues
121 contribute to dimerization. Taken together, our data reveal a wider range of oligomerization
122 states and functional activity in HKs than traditionally described.

123

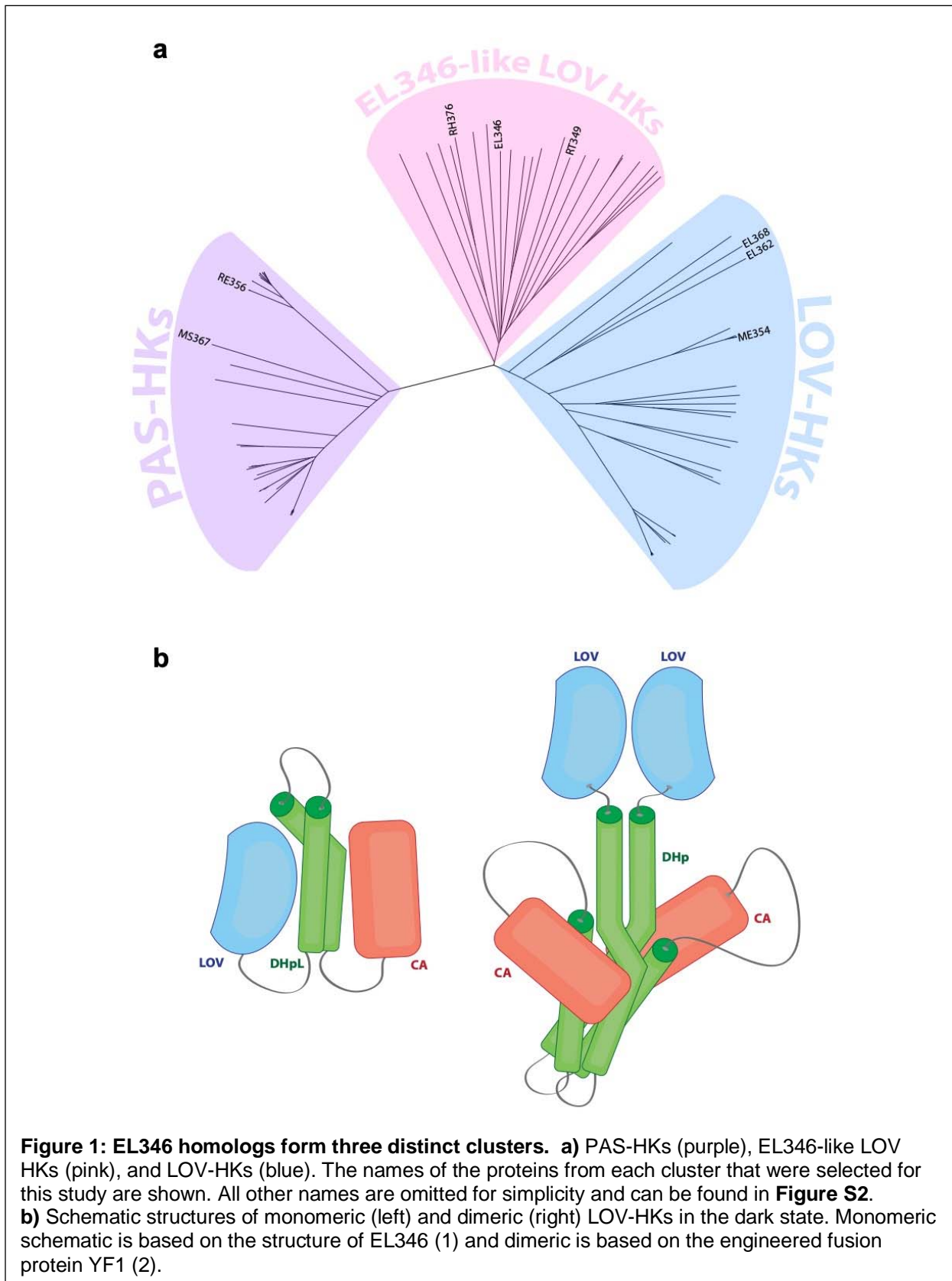
124 **Results**

125 ***Bioinformatics analysis reveals numerous alphaproteobacterial EL346 homologs***

126 To identify other potential monomeric histidine kinases, we searched for enzymes highly
127 similar in domain organization to the well-validated and functional EL346 monomer. In addition
128 to EL346, the top 100 BLASTp hits defined a set of proteins from *Alphaproteobacteria* which all
129 contained the same domain architecture of a single N-terminal PAS or LOV domain followed by
130 a C-terminal HWE/HisKA2 histidine kinase. None of these sequences contained any predicted

131 transmembrane segments, strongly suggesting all these candidates are soluble. A multiple
132 sequence alignment of these protein sequences and distance tree analysis revealed three
133 clusters (**Fig. 1a**), which split on increasingly diverse sensor types: EL346-like LOV-HKs, LOV-
134 HKs, and PAS-HKs (non-LOV). LOV domains were provisionally identified by the presence of
135 the characteristic “NCRFLQ” sequence and high homology (> 30% identity) to the EL346 LOV
136 domain (28), while the non-LOV PAS domains lacked this sequence motif (highlighted in **Fig.**
137 **S1**). Interestingly, a subgroup of the EL346-like LOV-HKs is missing the conserved
138 phosphoacceptor histidine (**Fig. S1**). We also included the previously-identified related EL368
139 (dimer) and EL362 (mixed oligomerization state) histidine kinases from *E. litoralis* HTCC2594
140 (20, 21), as well as the *Caulobacter crescentus* LovK (dimer) (29) in the alignment; all three of
141 these proteins grouped in the LOV-HKs cluster. Additionally, our search identified a third PAS-
142 HK cluster with proteins containing non-LOV PAS domains that shared 17-24% sequence
143 identity with the EL346 LOV domain. Notably, many of these domains contained a conserved
144 tryptophan in place of the cysteine utilized in LOV-type photochemistry (28) (**Fig. S1**). These
145 data show that the LOV/PAS-HK architecture is widespread throughout *Alphaproteobacteria* (as
146 are HWE/HisKA2 HKs in general (30, 31)) and contains members which could well respond to
147 stimuli other than blue light.

148



149 **LOV homologs are light sensing and appear mostly dimeric, but have diverse functional**
 150 **responses to illumination**

151 We posited that the EL346-like LOV-HK cluster might contain a mix of other monomeric
 152 and dimeric HKs, respectively analogous to EL346 and most natural HKs (as well as the
 153 engineered LOV-HK YF1 (2)), as illustrated in **Fig. 1b**. We selected several HKs from each
 154 cluster and characterized their oligomeric state and function with a variety of biochemical
 155 approaches. We started by determining the ability of the LOV-containing proteins to bind flavin
 156 chromophores and undergo typical LOV photochemistry via UV-visible absorbance
 157 spectroscopy. The absorbance spectra of dark and light state samples of four representative
 158 proteins – EL346, ME354, RT349, and RH376 (see **Table 1** for protein details) – all showed the

	Organism	Protein Name	Uniprot ID	% ID EL346	Condition	MW avg ± sd [max, min] (kDa)	Expected MW (kDa)	Oligomeric State
EL346-like LOV-HKs	<i>Erythrobacter litoralis</i> HTCC 2594	EL346	Q2NB77	100%	D +ATP	36.7 ± 3.0 [29.7, 39.3]	38.6/77.2	Monomer
					L +ATP	37.0 ± 1.9 [33.5, 38.8]		Monomer
	<i>Rubellimicrobium thermophilum</i> DSM 16684	RT349	S9SB69	41.6%	D +ATP	68.5 ± 1.5 [64.8, 70.6]	37.6/75.1	Mostly Dimer
					L +ATP	67.3 ± 1.4 [64.2, 69.1]		Mostly Dimer
	<i>Roseivivax halodurans</i> JCM 10272	RH376	X7EIB8	35.3%	D +ATP	81.5 ± 1.1 [78.7, 82.6]	42.5/85.0	Dimer
					L +ATP	80.8 ± 1.7 [76.4, 82.8]		Dimer
		RH1	N/A	N/A	D +ATP	86.6 ± 1.5 [84.3, 90.2]	42.1/84.1	Dimer
					L +ATP	80.8 ± 0.4 [79.8, 81.7]		Dimer
		RH2	N/A	N/A	D +ATP	73.2 ± 0.3 [72.1, 73.6]	41.8/83.5	Mostly Dimer
					L +ATP	74.9 ± 0.8 [73.5, 76.3]		Mostly Dimer
		RH3	N/A	N/A	D +ATP	76.4 ± 1.1 [74.8, 81.3]	39.5/78.9	Dimer
					L +ATP	76.5 ± 1.2 [74.9, 81.7]		Dimer
RH1+3	N/A	N/A	D +ATP	41.7 ± 1.8 [38.4, 46.8]	39.0/78.1	Mostly Monomer		
			L +ATP	48.1 ± 2.3 [44.2, 51.9]		Mostly Monomer		
LOV-HKs	<i>Methylorubrum extorquens</i> DM4	ME354	C7CCX6	27.7%	D +ATP	71.7 ± 3.1 [65.4, 74.8]	38.8/77.7	Mostly Dimer
				L +ATP	72.3 ± 4.0 [62.8, 75.6]	Mostly Dimer		
	<i>Erythrobacter litoralis</i> HTCC2594	EL368	Q4TL45	23.7%	N/A	N/A	N/A	N/A
<i>Erythrobacter litoralis</i> HTCC2594	EL362	Q2N9L9	22.3%	N/A	N/A	N/A	N/A	
PAS-HKs	<i>Rhizobium etli</i> CFM 42	RE356	Q2KD32	25.3%	Monomer	37.8 ± 0.7 [36.6, 38.6]	39.9/79.7	Monomer
					Dimer	87.4 ± 1.6 [84.6, 89.8]		Dimer
	<i>Methylocella silvestris</i> BL2	MS367	B8ELH4	26.0%	Monomer	38.3 ± 3.6 [32.7, 43.0]	40.2/80.4	Monomer
					Dimer	82.7 ± 6.4 [71.9, 96.7]		Dimer
Other	<i>Bacillus subtilis/ Bradyrhizobium japonicum</i>	YF1 (YtvA/FixL fusion)	N/A (PDB:4GCZ)	21.9%	N/A	N/A	N/A	Dimer

159
 160 **Table 1: Oligomeric states of known LOV-HKs and PAS-HKs include mix of monomers and dimers.**

161 Soluble HKs shown here are separated by cluster with the same coloring as Fig. 1 (EL346-like LOV HKs
 162 – pink, LOV-HKs – blue, PAS-HKs – purple, Other – grey) and include those investigated in this study
 163 (EL346, RT349, RH376, ME354, RE356, and MS367) as well as those identified in literature (EL368,
 164 EL362, and YF1) (2, 20). Mass data were collected using Superdex200 GL SEC-MALS (n=1). Values
 165 shown are MALS MW (average mass), minimum, maximum, and standard deviation among the points
 166 that make up the mass line for each measurement, and oligomeric states were defined using a qualitative
 167 five-bin scale.

168

169 characteristic flavin-LOV triplet (~450 nm) in the dark state which disappeared upon illumination
170 (**Fig. 2a**). Upon incubation in the dark, the 450 nm absorbance returned with first-order
171 exponential kinetics that varied by protein: the LOV-HKs measured here, such as ME354 (236
172 min), RT349 (240 min), and RH376 (62 min), had longer reversion constants τ than EL346 (33
173 min) (**Fig. 2b**). The particularly long reversion time constants of ME354 and RT349 can be
174 rationalized by the presence of several “slowing” mutations in their LOV domains relative to that
175 of EL346, specifically at positions 19, 21, 32, and 101 (EL346 numbering), as collated in a
176 review by Pudasaini and coworkers (**Fig S3**) (23).

177 We determined the oligomeric state of these LOV-HKs in the presence of ATP (1 mM) in
178 dark and light conditions using size exclusion chromatography coupled to multi-angle light
179 scattering (SEC-MALS). We began by confirming that EL346 is monomeric under both
180 conditions with minimal change in global shape upon illumination as revealed by SEC elution
181 profiles. In contrast, the three other LOV-HK proteins were dimeric or mostly dimeric, with
182 RT349 exhibiting a light-dependent shift in elution peak position and shape (**Fig. 2c, Table 1**).
183 Further investigation showed that the RT349 elution profile was also impacted by ATP as well:
184 in the absence of ATP, we observed two new peaks at even higher elution volumes in dark and
185 light conditions (**Fig. S4**).

186 While the oligomeric states of the three new LOV-HKs were all similar, analyses of
187 autophosphorylation activity indicated a diverse activity profile (**Fig. 3**). EL346 and RH376
188 exhibited the light-dependent increase in activity typically seen in LOV-HKs, albeit to different
189 extents. In contrast, RT349 displayed an inverted signaling logic, with higher
190 autophosphorylation rates in the dark state than in the light state. While this phenomenon has
191 been reported for engineered LOV-HKs such as YF1 variants (2) and the EL346 R175A mutant
192 (1), it does not seem to have been observed in a naturally-occurring LOV-HK. On the other end
193 of the spectrum, ME354 exhibited no detectable activity in both the dark and light, suggesting
194 that even though this protein properly photocycles, its kinase activity is not regulated directly by
195 light under these conditions. Overall, our results illustrate that despite adopting similar
196 oligomeric states, the LOV-HKs studied here exhibit diverse autophosphorylation activities,
197 suggesting varying forms of regulation and different signaling paradigms.

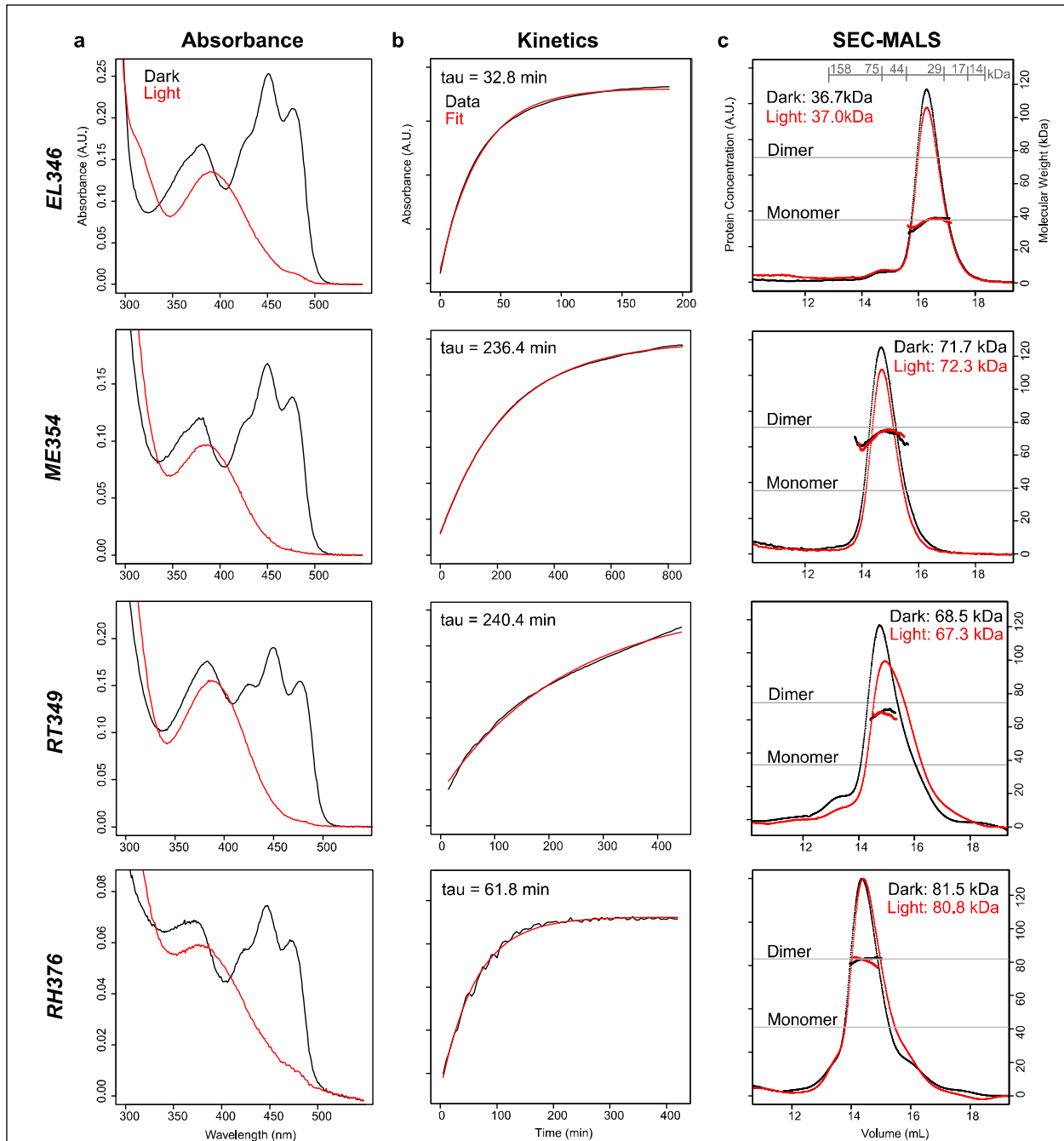
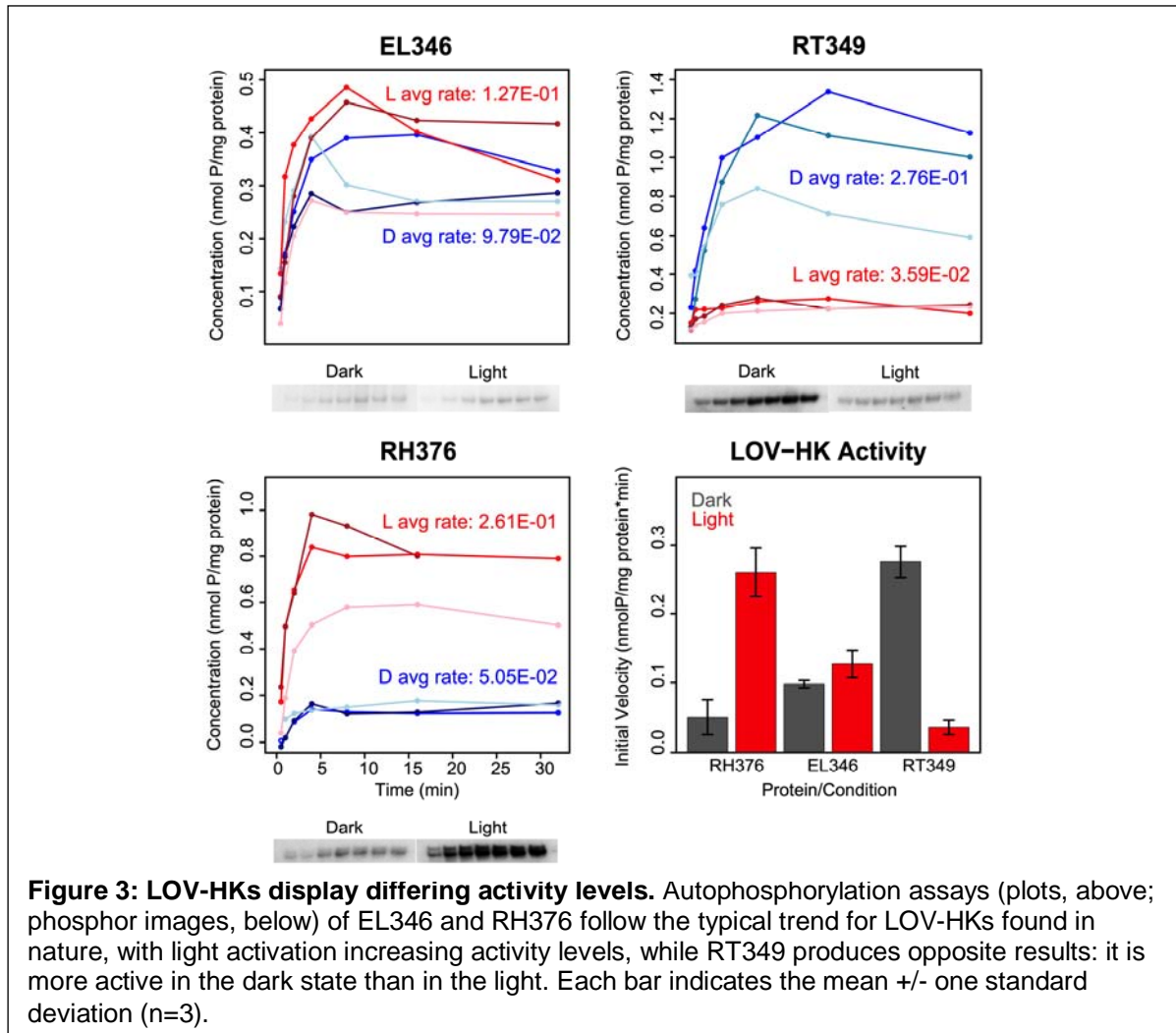


Figure 2: UV-visible absorption spectra and SEC-MALS reveal diversity of LOV-HK dark state reversion kinetics and oligomerization states. a) UV-visible absorption spectra of EL346, ME354, RT349, and RH376, superimposing dark state scans (black) with scans post-illumination (red). All spectra display the disappearance of the 450 nm triplet upon exposure to light, consistent with LOV photochemistry. Spectra were recorded in the presence of 1 mM ATP. **b)** Dark state reversion kinetics, measured by the return of absorbance at 446 nm post illumination (black), fit to single exponentials (red) reveal an 8-fold range of time constants. **c)** Superdex 200 GL SEC-MALS chromatograms are represented by dRI in arbitrary units and MALS-derived masses are solid lines under the peaks ($n=1$). MWs and elution volumes of six standard proteins are shown in grey in the top panel. MALS traces show that EL346 is monomeric in solution, while ME354, RT349 and RH376 are all predominantly dimeric (**Table 1**). A light-dependent shift in elution peak shape and position is seen in RT349.

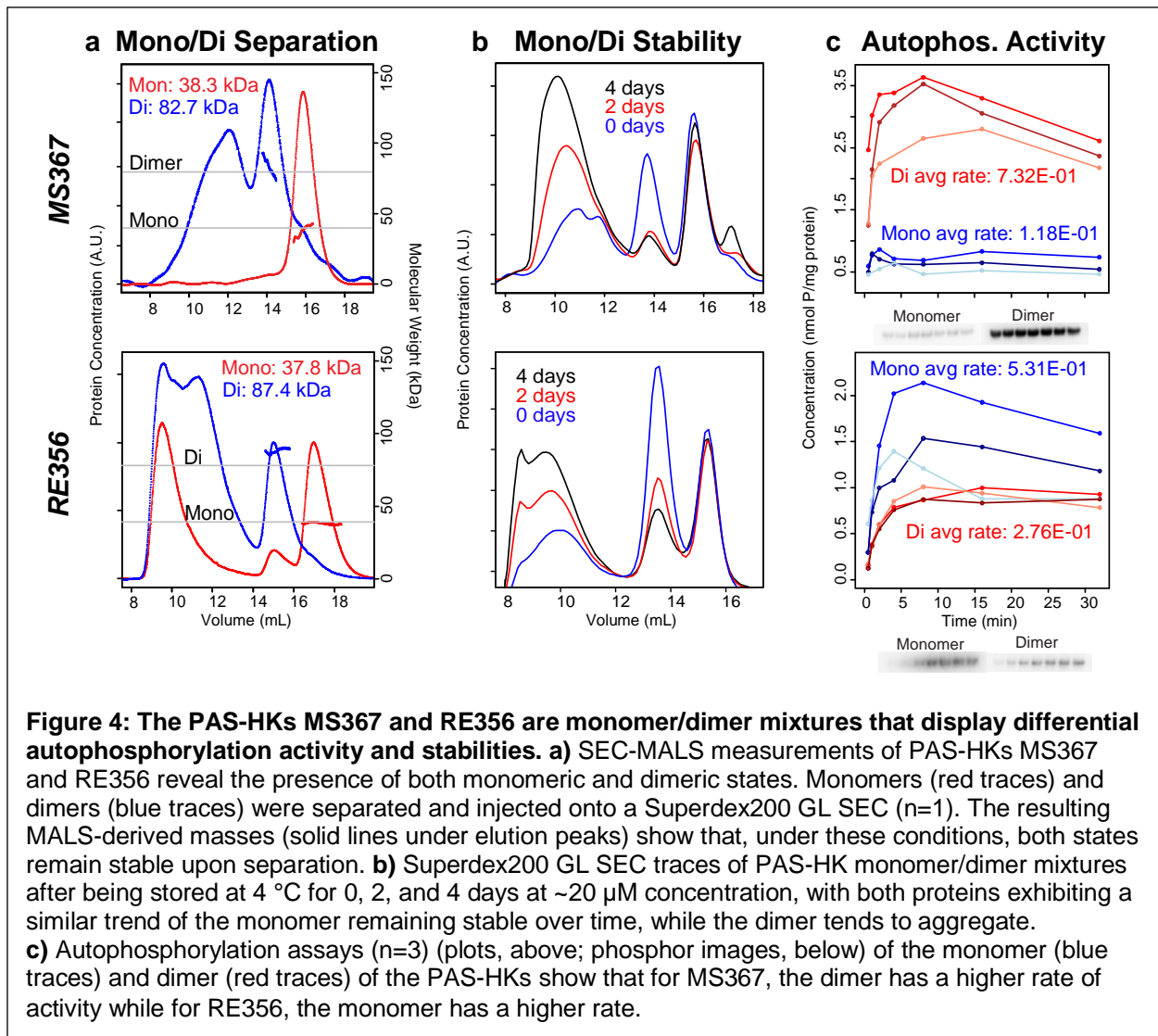


199

200

201 **Non-LOV PAS-HKs contain mixture of monomers and dimers, with each state exhibiting**
202 **different activity levels and stabilities**

203 The two PAS-HKs characterized here, from *Rhizobium etli* CFN 42 (RE356) and from
204 *Methylocella silvestris* BL2 (MS367), exhibit 45% sequence identity overall to one another (32%
205 over the PAS domain). In SEC-MALS experiments, both proteins appeared as mixtures of dimer
206 and monomer, as well as an oligomeric or aggregated fraction. We found that the monomeric
207 and dimeric states of MS367 and RE356 were in slow equilibrium, allowing them to be
208 separately purified and re-injected onto SEC-MALS (**Fig. 4a**). We characterized the *in vitro*
209 stability of the two different states by incubating mixed samples at 4°C for varying amounts of
210 time and using size-exclusion chromatography to visualize elution peaks. For both PAS-HKs,
211 we observed that the monomeric state was stable on the order of days, while the dimer slowly
212 oligomerized or aggregated on this timescale (**Fig. 4b**).



213

214

215 Though these proteins currently lack a known trigger analogous to light for the LOV-HKs,

216 we took advantage of the slow equilibrium between oligomeric states to determine whether they

217 exhibited differing levels of autophosphorylation. We observed that both MS367 and RE356

218 displayed autophosphorylation activity in their monomeric and dimeric states with the

219 characteristic plateau indicating an equilibrium between kinase and phosphatase activity (**Fig.**

220 **4c**). While the MS367 dimer appears to be more active than the monomer, RE356 produced

221 opposite results, with the monomer displaying more activity than the dimer. Despite similarity in

222 primary sequence and oligomeric assembly, the two PAS-HKs studied here in an *in vitro* context

223 have apparently opposite regulation via dimerization, again illustrating the diversity of function

224 across this family.

224

225 ***Engineering a “monomerized” LOV-HK***

226 Next, we sought to identify the determinants of dimerization in this family of sensor HKs,
227 recognizing that sequence changes can influence the multimeric arrangement of proteins
228 belonging to the same family (32, 33). To guide our analysis, we aligned the sequence of the
229 monomeric EL346 with those of selected dimeric HKs from all three clusters. These pairwise
230 alignments suggested four candidate regions that might influence dimerization; three regions
231 missing from EL346, but found in many of the other HKs (named RH1-3), as well a unique C-
232 terminal segment in EL346 (RH4) (**Figs. 5a and S5**).

233 To test the hypothesis that one or more of the RH1-4 regions might be determinants of
234 oligomeric state, we systematically deleted one or more of these regions from the dimeric
235 RH376 protein, which contained all four segments, in the hope of finding a constitutively
236 monomeric variant (**Figs. 5b and 5c**). As the RH4 segment corresponds almost entirely to the
237 highly dynamic C-terminal residues we previously deleted without effect on the monomeric state
238 of EL346 (18), we did not investigate RH4 as a driver of monomer/dimer state and instead
239 focused on the RH1-3 segments unique to RH376.

240 Observing that the insert regions were either in previously-reported dimerization
241 interfaces for LOV domains (RH1, A' α helix) (2, 20, 34) and HKs (RH2, DHp domain) (35, 36),
242 or large insertions with predicted secondary structure elements (RH3, ATP lid), we hypothesized
243 that these segments could contribute to the dimerization of RH376 and perhaps other HKs. A
244 RH376 homology model (37) based on the engineered dimeric LOV-HK YF1 protein (2)
245 illustrates the potential involvement of these residues in dimerization interfaces (**Fig. 5c**). We
246 thus deleted each of the RH1, RH2, and RH3 regions from the RH376 sequence both
247 individually and in combination, expressed these variant proteins, and compared them to RH376
248 WT in terms of LOV photocycle, oligomeric state, and autophosphorylation activity.

249

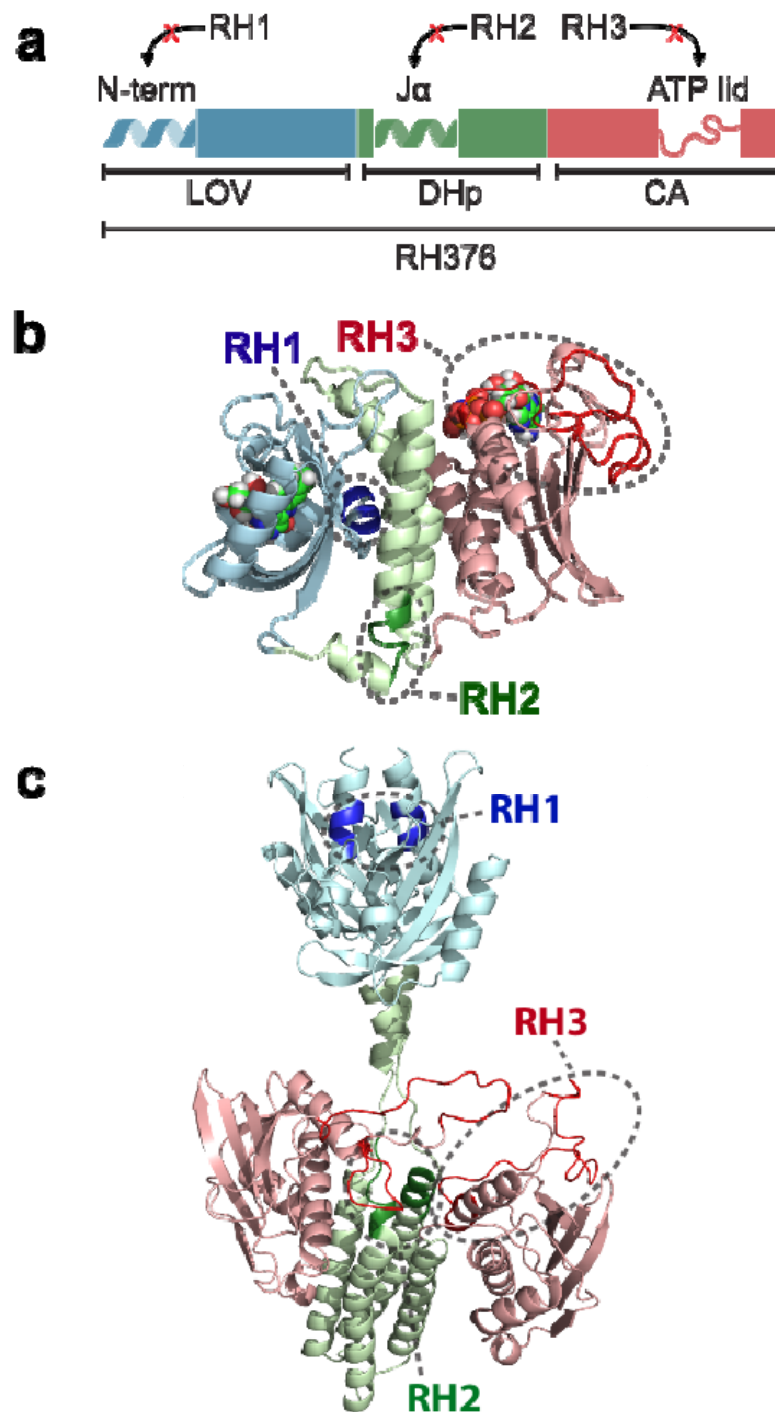


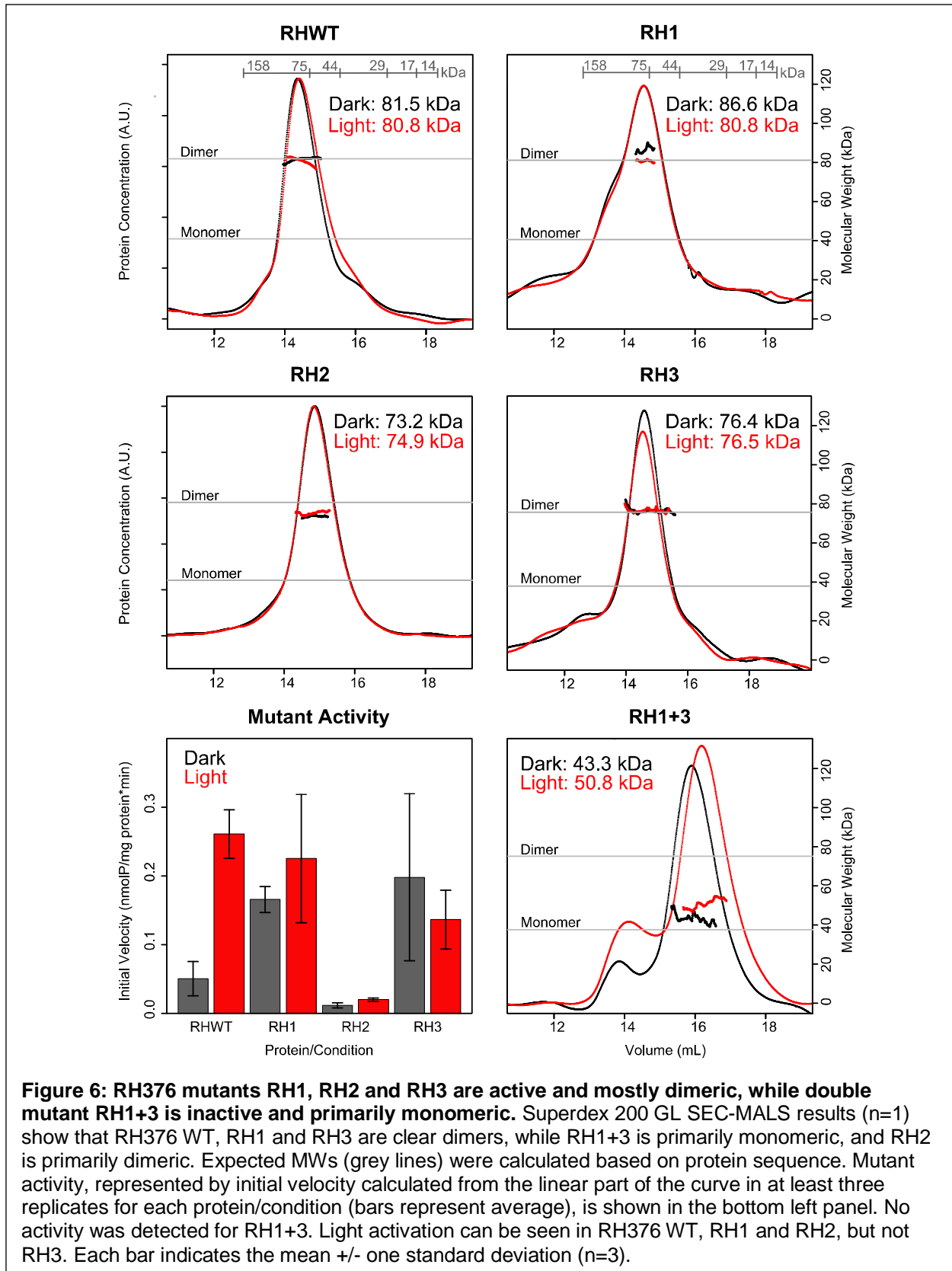
Figure 5: RH376 mutant deletion regions are designed in predicted dimer interfaces. RH376 deletion mutants RH1, RH2, and RH3 are highlighted in 3 schematics: **a)** Domain architecture with the predicted secondary structure at the location of each deletion. RH1 is located in the A'α helix of the LOV domain, RH2 in the linker between the LOV domain and α1 of the DHp domain, and RH3 is in the ATP lid. **b)** Monomeric homology model of RH376 based on the structure of EL346 (1). **c)** Dimeric homology model of RH376 based on the engineered YF1 sensor kinase (2). All LOV domains are colored blue, DHp domains green, and CA domains red. Mutations are highlighted and circled.

251 RH1, RH2, and RH3 proteins displayed the characteristic LOV absorbance triplet
252 centered at 450 nm and exhibited dark state reversion kinetics similar to the WT protein (**Fig.**
253 **S6**), suggesting that the deletions did not perturb the folding and function of the LOV domain. In
254 RH2, we detected a small change in the relative heights of the triplet peaks, indicating that flavin
255 binding is likely adversely affected (**Fig. S6**) despite the deletion occurring outside the LOV
256 domain. We determined the oligomeric state of each deletion mutant by SEC-MALS; while none
257 of the single deletion constructs eluted as a monomer regardless of dark or light conditions,
258 RH2 had an altered measured mass and SEC elution volume which suggest it samples both
259 dimeric and monomeric conformations (**Table 1, Fig. 6**).

260 We suspected that none of these deletions would have a major impact on
261 autophosphorylation activity of RH376, given their modest effects on photocycle and
262 oligomerization state. As a baseline, we found that the RH376 WT protein displays robust
263 autophosphorylation activity in the dark as well as a ~5x increase in initial velocity upon
264 illumination (**Table S1, Fig. 6**). The RH1 mutant showed autophosphorylation activity similar to
265 the WT in the light, but greater in the dark, resulting in a much lower degree of light-activation.
266 Similarly, RH2 retained some light activation, but showed very little activity in both dark and light
267 conditions (**Table S1, Fig. 6**). On the other hand, RH3 displayed activity in the dark that was
268 ~4x the WT initial velocity, with a light-dependent decrease in activity (**Table S1, Fig. 6**). In all,
269 each mutant had a markedly different effect on autophosphorylation activity despite having
270 minimal effects on dimerization.

271 Given that neither RH1 nor RH3 perturbed dimeric state and both displayed activity
272 levels comparable to WT, yet had divergent effects on light-activation (**Table S1, Fig. 6**), we
273 explored the effects of combining these deletions ("RH1+3"). While neither the LOV absorbance
274 spectrum nor photocycle of this protein were affected (**Fig. S6**), SEC-MALS showed a dramatic
275 change in oligomeric state, as RH1+3 existed mainly as a monomer, though neither deletion
276 alone showed monomeric character (**Table S1, Fig. 6**). Additionally, we detected no
277 autophosphorylation activity in RH1+3 at conditions similar to the other proteins tested. Overall,
278 we conclude that RH376 uses a distributed set of residues to control oligomeric state.

279



281 Discussion

282 Our work further expands the known behavior of sensor HKs to include two proteins in
283 slow monomer:dimer equilibria along with three chiefly dimeric proteins, one of which exhibits a
284 slight conformational change upon activation, and all of which exhibit varying activities. Prior to
285 this study, the vast majority of characterized sensor HKs were dimers with the EL346 LOV-HK
286 from *E. litoralis* HTCC2594 (1, 20) as the only well-characterized, functional protein that we are
287 aware of as an exclusive monomer. Using sequence homology searches to find homologs of
288 EL346, we found a large family of related LOV- and PAS-HKs in the *Alphaproteobacteria*. Most
289 of these proteins were Pfam (19) HisKA_2 or HWE-HK-type histidine kinases, two groups of
290 HKs that have been less well-characterized structurally to date (1, 12, 14, 38), and we
291 hypothesized that a subset of these sequences with the highest homology to monomeric EL346
292 might contain other monomers.

293 Contrary to this expectation, we found a diverse range of assemblies, conformational
294 changes, and autophosphorylation activity among the five new sensor HKs characterized here.
295 For the LOV-HK proteins, we found several dimers, including two members of the EL346-like
296 cluster of LOV-HKs (RT349 and RH376) which SEC-MALS analyses showed to be dimeric or
297 primarily dimeric in both dark and light conditions. ME354, a newly characterized member of the
298 other LOV-HK cluster is also mostly dimeric, similar to the established EL368 and *C. crescentus*
299 LovK (20, 29), which both also cluster within that second group.

300 While these new LOV-HKs are all mostly dimeric, we observed differences in their
301 structural response to blue light activation as assessed by SEC-MALS: ME354 and RH376
302 showed minimal light-dependent change, while RT349 eluted at later volumes in the light,
303 suggesting that it adopts a more compact structure under this condition. Notably, this shift was
304 dependent upon not only light, but also the presence of ATP (**Fig. S4**). These light-dependent
305 changes are more substantial than we previously observed by SEC-MALS with the EL346 and
306 EL368 LOV-HKs (1, 18, 20), and are perhaps similar to the kinds of changes seen by small

307 angle solution X-ray scattering in the engineered YF1 protein (2, 39). Further studies are
308 needed to more fully characterize these motions and establish how they relate to the large
309 conformational changes postulated to accompany activation from crystal structures of inactive
310 HKs (40, 41). RT349 is also very distinctive in that it is more active in the dark than in the light
311 **(Fig. 3)**. While this behavior has been observed before in variants of engineered (2) and
312 mutants of natural LOV-HKs (1), we are not aware of any naturally-occurring LOV-HKs that
313 share this signaling polarity. We anticipate that such a light-dependent change in net
314 autophosphorylation has contributions from altered kinase and phosphatase activities (42), and
315 this will be the focus of a subsequent investigation.

316 Turning to the two PAS-HKs, both RE356 and MS367 interconvert slowly enough
317 between dimeric and monomeric states that we could separate them by size exclusion
318 chromatography. We observed differing activity levels of the various oligomerization states of
319 these proteins – both monomers are active, with the MS367 dimer being more active than the
320 monomer, and RE356 displaying opposite results **(Fig. 4)**. The *in vitro* data lead us to propose a
321 mechanism where shifts in the monomer:dimer equilibrium could regulate sensor HK enzymatic
322 activity. While demonstrating that monomer:dimer control of RE356 and MS367 activity *in vivo* is
323 outside the scope of this work, we note that comparable mechanisms are widely accepted or
324 suggested for a very broad range of signaling proteins including certain sensor HKs (43),
325 receptor tyrosine kinases (44), and photoreceptors (45-48). In this case, dimerization may be
326 modulated by potential ligand binding in the yet-uncharacterized PAS domains of these HKs, as
327 in other PAS-domain containing signaling proteins (49), or via other mechanisms. Perhaps the
328 relative instability of the dimer state, which forms higher-molecular-weight aggregates over time,
329 could serve as an intrinsic timer specifically on one of the two signaling species to temporally
330 modify a biological response post-activation.

331 Given the integral role of dimerization for many sensor HKs, we sought to understand
332 the sequence determinants of dimerization with an engineering approach. Using RH376 as a

333 model dimer, we systematically removed combinations of the three insertions it contains
334 compared to the monomeric EL346 (**Fig. 5, S5**), hypothesizing that one or more of these
335 changes could create a monomeric LOV-HK. While each deletion mutant was well-folded as
336 evidenced by binding flavin chromophores and undergoing canonical LOV photochemistry, we
337 found that all three single deletion mutants (RH1, RH2, RH3) remained largely dimeric despite
338 the removal of 5-30 amino acid residues apiece. Remarkably, the combination of two of these
339 deletions to generate the RH1+3 construct substantially monomerized the protein and abolished
340 autophosphorylation activity.

341 From these studies on RH376, we arrive at the general conclusion that multiple regions
342 determine oligomeric states in this family of LOV-HKs. The use of distributed interfaces for
343 dimerization is consistent with structural studies on the dimeric YF1 engineered sensor kinase
344 (2) showing intermonomer contacts via both the LOV and DHP domains, which are typical
345 dimerization interfaces for LOV photosensors (2, 50) and canonical HisKA histidine kinases (13,
346 51) respectively. These correspond to our RH1 and RH2 deletions; neither of these changes,
347 nor the RH3 deletion in a large loop near the kinase ATP binding site, were sufficient on its own
348 to generate monomers. Unexpectedly, the RH3 deletion – which removes a large loop near the
349 ATP binding site – affected dimerization when paired with RH1. While this site has not been
350 previously described as being involved in dimerization to the best of our knowledge, we note
351 that ATP itself bridges interactions between multiple domains in two known HWE/HisKA2 HK
352 crystal structures (1, 38), laying some precedent for interactions at or near the nucleotide to be
353 involved in dimerization. Clearly, further structural work is needed to more fully assess how
354 dimerization is encoded among multiple HKs.

355 The diversity of oligomeric states and function in a family of sensor HKs that we
356 uncovered here opens the door to novel regulatory modes within this family, such as control of
357 dimerization, whether by ligand or inherent thermodynamic stability, or cooperativity. The closely
358 related bacterial chemoreceptor proteins, for instance, form large arrays to increase signaling

359 output through cooperativity (16). Similar use of monomer/dimer transitions and evolution of
360 variable quaternary structure is at the heart of acquiring cooperativity and novel regulatory
361 modes in the classic hemoglobin family of oxygen-binding proteins, which started as ancestral
362 monomers prior to dimerizing by gene duplication events and the acquisition of a relatively small
363 number of mutations (33). Our findings suggest that various oligomeric states within the sensor
364 HK family could allow for different potential for cooperativity, perhaps depending on the input
365 signal or output pathway, or integrating multiple points of control or regulation to be added to the
366 canonical signal transduction pathway of two-component systems.

367

368 **Experimental Procedures**

369 ***Bioinformatics***

370 Sequences similar to EL346 were identified by a BLAST search with default parameters
371 against the non-redundant NCBI database, using EL346 full-length protein sequence (Uniprot
372 ID: Q2NB77) as a query. EL346 and the best 100 hits were aligned using Clustal Omega (52)
373 and a distance tree was calculated from this alignment using the same software. Graphic
374 display of this tree was accomplished using iTOL (Interactive Tree of Life, <http://itol.embl.de/>)
375 (53). This tree was used to select HKs for cloning from the strains available at DSMZ
376 (<http://www.dsmz.de>).

377

378 ***Cloning, protein expression and purification***

379 Five HKs were selected for biochemical characterization, abbreviated RT349, RH376,
380 ME354, RE356, and MS367 from the combination of their species name (e.g. *Rubellimicrobium*
381 *thermophilum* = RT) and number of amino acid residues (**Table 1**). DNA encoding these
382 proteins were cloned into a pHis-G β 1 vector (54), with constructs verified by DNA sequencing.
383 Proteins were overexpressed in *Escherichia coli* BL21(DE3) (Stratagene) in LB as previously
384 described (18). Cells were harvested, resuspended in Buffer A (50 mM Tris pH 8.0, 100 mM

385 NaCl, and 10 mM MgCl₂), and lysed by sonication. Lysates were centrifuged at 48,000 x g and
386 4 °C for 45 min. Supernatants were loaded into a Ni²⁺ Sepharose affinity column (GE
387 Healthcare) and the His₆-Gβ1 tagged protein was washed with 4 column volumes of Buffer A
388 supplemented with 15 mM imidazole and eluted with 4 column volumes of Buffer A
389 supplemented with 250 mM imidazole. Eluted proteins were exchanged into Buffer A by dialysis,
390 then fusion tags were cleaved by incubation with His₆-TEV protease overnight at 4 °C. The tag-
391 less proteins were separated from the tags and His₆-TEV protease by Ni²⁺ affinity
392 chromatography and were further purified by size-exclusion chromatography on a HiLoad
393 16/600 Superdex 200 column (GE Healthcare) equilibrated with HSEC buffer containing 50 mM
394 HEPES pH 7.5, 100 mM NaCl, 10 mM MgCl₂, and 0.5 mM DTT. For light-sensitive proteins, all
395 purification steps were performed under dim red light. Concentrations were determined from the
396 theoretical absorption coefficient, ϵ_{280} for PAS-HKs, calculated from the sequence using the
397 ExPASy ProtParam server (55), and $\epsilon_{446} = 11,800 \text{ M}^{-1} \text{ cm}^{-1}$ for flavin-containing proteins.

398 RH376 deletion mutants were generated as follows: RH2 and RH3 were ordered as
399 synthetic constructs from Genewiz (South Plainfield, NJ) and inserted into the same pHis-Gβ1
400 vector as the WT protein. RH1 and RH1+3 mutants were generated by PCR using an N-
401 terminal primer lacking the sequence to be deleted using WT and RH3 plasmids as templates,
402 respectively.

403

404 ***Absorbance and dark state reversion kinetics***

405 UV-visible absorbance spectroscopy measurements were acquired using a Varian Cary
406 50 spectrophotometer at 24 °C with a 1 cm path length quartz cuvette. First, a UV-visible
407 spectrum in the range 250-550 nm was acquired in light and dark conditions for each LOV-HK.
408 For dark measurements, all steps were performed under dim red light. For light measurements,
409 the samples were illuminated for 1 minute using a blue LED panel (225 LED bulbs in 30.5 ×

410 30.5-cm panel, 13.8 W, 465 nm maximum illumination wavelength; LEDwholesalers [Hayward,
411 CA]) prior to each scan. To measure dark state recovery, each LOV-HK sample was illuminated
412 under a blue LED panel for 1 minute and then transferred to the spectrophotometer. A_{446} of the
413 samples in HSEC buffer with 1 mM ATP was monitored at 5-min intervals for 400-800 min at
414 24 °C. Time constants τ were determined by fitting measurements to a monoexponential decay
415 using the following equation:

$$416 \quad \text{Abs} = A_{\text{inf}} - (A_{\text{inf}} - A_0)e^{-t/\tau}, \text{ where } A_{\text{inf}} = A_{446} \text{ at infinity, } A_0 = A_{446} \text{ initial, and } t = \text{time}$$

417 Raw data were fit and plotted using RStudio with the nls function; plots were edited in Adobe
418 Illustrator CS6.

419

420 **SEC-MALS**

421 All samples and buffers were filtered with a 0.1- μm pore size filter before use. ATP was
422 added to each HK sample (~15 μM , 400 μL) to a final concentration of 1 mM. Samples were
423 then injected at a 0.4 mL/min flow rate onto a Superdex 200 GL 10/300 (or in the case of Figure
424 S4, Superdex 200 Increase GL 10/300) SEC column (GE Healthcare) using HSEC buffer with 1
425 mM ATP. For lit experiments, samples were illuminated with a blue LED panel for 1 min prior to
426 injection and the blue LED panel was faced toward the column during the run. For dark
427 experiments, all steps were performed under dim red light. Samples were detected post-elution
428 by the inline miniDAWN TREOS light scattering and Optilab rEX refractive index detectors
429 (Wyatt Technology [Santa Barbara, CA]). FPLC runs were performed at 4 °C, while MALS and
430 refractive index measurements were at 25 °C. Data analysis and molecular weight calculations
431 were performed using the ASTRA V software (Wyatt Technology). Raw data were plotted using
432 RStudio. Assignments of oligomeric state are based on a qualitative, five-bin scale, with proteins
433 considered to be “dimeric” or “monomeric” when their MALS-calculated mass falls within $\pm 5\%$ of

434 the sequence-derived molecular weight for either state. Between these ranges are three bins of
435 equal size: “mostly dimer”, “monomer/dimer mixture”, and “mostly monomer.”

436

437 ***Autophosphorylation assays***

438 Autophosphorylation was measured as described previously (1, 18). A minimum of three
439 trials were conducted for each protein under each condition. Proteins were added to a reaction
440 buffer containing 50 mM Tris, 100 mM NaCl, 5 mM MnCl₂, and 1 mM DTT with pH 8.2. Protein
441 concentrations were confirmed by analysis of dilution series on Coomassie-stained SDS-PAGE.
442 Final reaction concentrations ranged from approximately 10 to 35 micromolar as listed in the
443 table below:

444

<i>Protein</i>	<i>Concentration (μM)</i>	<i>Protein</i>	<i>Concentration (μM)</i>
EL346	16.1	RE356 monomer	9.6
ME354	11.6	RE356 dimer	8.5
RT349	28.6	RH1	12.4
RH376 WT	14.3	RH2	30.4
MS367 monomer	10.7	RH3	34.7
MS367 dimer	11.1	RH1+3	9.1

445

446 A mixture of unlabeled ATP and 10 μCi [γ -³²P] ATP was added to each mixture to initiate
447 the reaction (final ATP concentration of 200 μM). Aliquots were removed at time points of 0.5, 1,
448 2, 4, 8, 6, and 32 min and placed into a 4x SDS-gel loading buffer to quench the reaction. For
449 dark measurements, all steps were performed under dim red light. For light measurements, the
450 samples were illuminated with a blue LED panel just prior to and throughout the course of the

451 experiment. Samples were subjected to SDS-PAGE analysis; dried gels were exposed for 1 hr -
452 overnight and bands were visualized by phosphorimaging. Band intensities were measured
453 using Fiji (56, 57); initial velocity values were calculated in Microsoft Excel from the linear region
454 of the curve and were plotted in RStudio.

455

456 *Data availability* – All data for this work are contained in this manuscript.

457

458 *Supporting information* – This article contains supporting information, including Figures S1-6,
459 Table S1, and accompanying literature citations.

460

461 *Acknowledgements* – The authors would like to acknowledge Bright Shi for generating the
462 RH1+3 construct, as well as Matthew Cleere, Zaynab Jaber, Jaynee Hart, and other Gardner
463 lab members for fruitful discussions.

464

465 *Funding and additional information* – This work was supported by NIH grants R01 GM106239
466 (to K.H.G.) and F32 GM1119311 (to I.D.). The content is solely the responsibility of the authors
467 and does not necessarily represent the official views of the National Institutes of Health.

468

469 *Conflict of interest* – The authors declare that they have no conflicts of interest with the contents
470 of this article.

471

472 *Abbreviations* –HK, histidine kinase; LOV, Light-Oxygen-Voltage; PAS, Per-ARNT-Sim; TCS,
473 two-component system; RR, response regulator; DHp, dimerization histidine phosphotransfer;
474 CA, catalytic ATP-binding; SEC-MALS, size exclusion chromatography multi-angle light
475 scattering.

476

477 **References**

- 478 1. Rivera-Cancel, G., Ko, W. H., Tomchick, D. R., Correa, F., and Gardner, K. H. (2014)
479 Full-length structure of a monomeric histidine kinase reveals basis for sensory regulation
480 Proc Natl Acad Sci U S A **111**, 17839-17844 10.1073/pnas.1413983111
- 481 2. Diensthuber, R. P., Bommer, M., Gleichmann, T., and Moglich, A. (2013) Full-length
482 structure of a sensor histidine kinase pinpoints coaxial coiled coils as signal transducers
483 and modulators Structure **21**, 1127-1136 10.1016/j.str.2013.04.024
- 484 3. Galperin, M. Y. (2018) What bacteria want Environmental microbiology **20**, 4221-4229
485 10.1111/1462-2920.14398
- 486 4. Mascher, T., Helmann, J. D., and Uden, G. (2006) Stimulus perception in bacterial
487 signal-transducing histidine kinases Microbiol Mol Biol Rev **70**, 910-938
488 10.1128/MMBR.00020-06
- 489 5. West, A. H., and Stock, A. M. (2001) Histidine kinases and response regulator proteins
490 in two-component signaling systems Trends Biochem Sci **26**, 369-376,
491 <https://www.ncbi.nlm.nih.gov/pubmed/11406410>
- 492 6. Wang, S. (2012) Bacterial Two-Component Systems: Structures and Signaling
493 Mechanisms In Protein Phosphorylation in Human Health, Huang C, ed. InTech, Chapter
494 15,
- 495 7. Mechaly, A. E., Soto Diaz, S., Sassoon, N., Buschiazzo, A., Betton, J. M., and Alzari, P.
496 M. (2017) Structural Coupling between Autokinase and Phosphotransferase Reactions
497 in a Bacterial Histidine Kinase Structure **25**, 939-944 e933 10.1016/j.str.2017.04.011
- 498 8. Kenney, L. J., and Anand, G. S. (2020) EnvZ/OmpR Two-Component Signaling: An
499 Archetype System That Can Function Noncanonically EcoSal Plus **9**,
500 10.1128/ecosalplus.ESP-0001-2019

- 501 9. Bhate, M. P., Molnar, K. S., Goulian, M., and DeGrado, W. F. (2015) Signal transduction
502 in histidine kinases: insights from new structures *Structure* **23**, 981-994
503 10.1016/j.str.2015.04.002
- 504 10. Szurmant, H., White, R. A., and Hoch, J. A. (2007) Sensor complexes regulating two-
505 component signal transduction *Curr Opin Struct Biol* **17**, 706-715
506 10.1016/j.sbi.2007.08.019
- 507 11. Gushchin, I., and Gordeliy, V. (2018) Transmembrane Signal Transduction in Two-
508 Component Systems: Piston, Scissoring, or Helical Rotation? *Bioessays* **40**,
509 10.1002/bies.201700197
- 510 12. Rinaldi, J., Fernandez, I., Shin, H., Sycz, G., Gunawardana, S., Kumarapperuma, I. *et al.*
511 (2021) Dimer Asymmetry and Light Activation Mechanism in *Brucella* Blue-Light Sensor
512 Histidine Kinase *mBio* **12**, 10.1128/mBio.00264-21
- 513 13. Ashenberg, O., Keating, A. E., and Laub, M. T. (2013) Helix bundle loops determine
514 whether histidine kinases autophosphorylate in cis or in trans *J Mol Biol* **425**, 1198-1209
515 10.1016/j.jmb.2013.01.011
- 516 14. Herrou, J., Crosson, S., and Fiebig, A. (2017) Structure and function of HWE/HisKA2-
517 family sensor histidine kinases *Curr Opin Microbiol* **36**, 47-54 10.1016/j.mib.2017.01.008
- 518 15. Luo, B. H., Carman, C. V., and Springer, T. A. (2007) Structural basis of integrin
519 regulation and signaling *Annual review of immunology* **25**, 619-647
520 10.1146/annurev.immunol.25.022106.141618
- 521 16. Muok, A. R., Briegel, A., and Crane, B. R. (2020) Regulation of the chemotaxis histidine
522 kinase CheA: A structural perspective *Biochimica et biophysica acta Biomembranes*
523 **1862**, 183030 10.1016/j.bbamem.2019.183030
- 524 17. Kitayama, Y., Nishiwaki-Ohkawa, T., and Kondo, T. (2014) Intersubunit communications
525 within KaiC hexamers contribute the robust rhythmicity of the cyanobacterial circadian
526 clock *Microb Cell* **1**, 67-69 10.15698/mic2014.01.129

- 527 18. Dikiy, I., Edupuganti, U. R., Abzalimov, R. R., Borbat, P. P., Srivastava, M., Freed, J. H.
528 *et al.* (2019) Insights into histidine kinase activation mechanisms from the monomeric
529 blue light sensor EL346 Proc Natl Acad Sci U S A **116**, 4963-4972
530 10.1073/pnas.1813586116
- 531 19. El-Gebali, S., Mistry, J., Bateman, A., Eddy, S. R., Luciani, A., Potter, S. C. *et al.* (2019)
532 The Pfam protein families database in 2019 Nucleic Acids Res **47**, D427-D432
533 10.1093/nar/gky995
- 534 20. Correa, F., Ko, W. H., Ocasio, V., Bogomolni, R. A., and Gardner, K. H. (2013) Blue light
535 regulated two-component systems: enzymatic and functional analyses of light-oxygen-
536 voltage (LOV)-histidine kinases and downstream response regulators Biochemistry **52**,
537 4656-4666 10.1021/bi400617y
- 538 21. Swartz, T. E., Tseng, T. S., Frederickson, M. A., Paris, G., Comerci, D. J., Rajashekara,
539 G. *et al.* (2007) Blue-light-activated histidine kinases: two-component sensors in bacteria
540 Science **317**, 1090-1093 10.1126/science.1144306
- 541 22. Crosson, S., Rajagopal, S., and Moffat, K. (2003) The LOV domain family:
542 photoresponsive signaling modules coupled to diverse output domains Biochemistry **42**,
543 2-10 10.1021/bi026978l
- 544 23. Pudasaini, A., El-Arab, K. K., and Zoltowski, B. D. (2015) LOV-based optogenetic
545 devices: light-driven modules to impart photoregulated control of cellular signaling Front
546 Mol Biosci **2**, 18 10.3389/fmolb.2015.00018
- 547 24. Gao, R., and Stock, A. M. (2009) Biological insights from structures of two-component
548 proteins Annu Rev Microbiol **63**, 133-154 10.1146/annurev.micro.091208.073214
- 549 25. Tseng, T. S., Frederickson, M. A., Briggs, W. R., and Bogomolni, R. A. (2010) Light-
550 activated bacterial LOV-domain histidine kinases Methods Enzymol **471**, 125-134
551 10.1016/S0076-6879(10)71008-9

- 552 26. Möglich, A. (2019) Signal transduction in photoreceptor histidine kinases *Protein Sci* **28**,
553 1923-1946 10.1002/pro.3705
- 554 27. Zoltowski, B. D., and Gardner, K. H. (2011) Tripping the light fantastic: blue-light
555 photoreceptors as examples of environmentally modulated protein-protein interactions
556 *Biochemistry* **50**, 4-16 10.1021/bi101665s
- 557 28. Crosson, S., and Moffat, K. (2001) Structure of a flavin-binding plant photoreceptor
558 domain: insights into light-mediated signal transduction *Proc Natl Acad Sci U S A* **98**,
559 2995-3000 10.1073/pnas.051520298
- 560 29. Purcell, E. B., McDonald, C. A., Palfey, B. A., and Crosson, S. (2010) An analysis of the
561 solution structure and signaling mechanism of LovK, a sensor histidine kinase
562 integrating light and redox signals *Biochemistry* **49**, 6761-6770 10.1021/bi1006404
- 563 30. Karniol, B., and Vierstra, R. D. (2004) The HWE histidine kinases, a new family of
564 bacterial two-component sensor kinases with potentially diverse roles in environmental
565 signaling *J Bacteriol* **186**, 445-453, <https://www.ncbi.nlm.nih.gov/pubmed/14702314>
- 566 31. Staroń, A., and Mascher, T. (2010) General stress response in alpha-proteobacteria:
567 PhyR and beyond *Mol Microbiol* **78**, 271-277 10.1111/j.1365-2958.2010.07336.x
- 568 32. Perica, T., Chothia, C., and Teichmann, S. A. (2012) Evolution of oligomeric state
569 through geometric coupling of protein interfaces *Proc Natl Acad Sci U S A* **109**, 8127-
570 8132 10.1073/pnas.1120028109
- 571 33. Pillai, A. S., Chandler, S. A., Liu, Y., Signore, A. V., Cortez-Romero, C. R., Benesch, J.
572 L. P. *et al.* (2020) Origin of complexity in haemoglobin evolution *Nature* **581**, 480-485
573 10.1038/s41586-020-2292-y
- 574 34. Banerjee, A., Herman, E., Kottke, T., and Essen, L. O. (2016) Structure of a Native-like
575 Aureochrome 1a LOV Domain Dimer from *Phaeodactylum tricornutum* *Structure* **24**,
576 171-178 10.1016/j.str.2015.10.022

- 577 35. Qin, L., Dutta, R., Kurokawa, H., Ikura, M., and Inouye, M. (2000) A monomeric histidine
578 kinase derived from EnvZ, an Escherichia coli osmosensor Mol Microbiol **36**, 24-32,
579 <https://www.ncbi.nlm.nih.gov/pubmed/10760160>
- 580 36. Tomomori, C., Tanaka, T., Dutta, R., Park, H., Saha, S. K., Zhu, Y. *et al.* (1999) Solution
581 structure of the homodimeric core domain of Escherichia coli histidine kinase EnvZ Nat
582 Struct Biol **6**, 729-734 10.1038/11495
- 583 37. Waterhouse, A., Bertoni, M., Bienert, S., Studer, G., Tauriello, G., Gumienny, R. *et al.*
584 (2018) SWISS-MODEL: homology modelling of protein structures and complexes
585 Nucleic Acids Research **46**, W296-W303 10.1093/nar/gky427
- 586 38. Rinaldi, J., Arrar, M., Sycz, G., Cerutti, M. L., Berguer, P. M., Paris, G. *et al.* (2016)
587 Structural Insights into the HWE Histidine Kinase Family: The Brucella Blue Light-
588 Activated Histidine Kinase Domain J Mol Biol **428**, 1165-1179
589 10.1016/j.jmb.2016.01.026
- 590 39. Berntsson, O., Diensthuber, R. P., Panman, M. R., Bjorling, A., Hughes, A. J., Henry, L.
591 *et al.* (2017) Time-Resolved X-Ray Solution Scattering Reveals the Structural
592 Photoactivation of a Light-Oxygen-Voltage Photoreceptor Structure **25**, 933-938 e933
593 10.1016/j.str.2017.04.006
- 594 40. Mechaly, A. E., Sassoon, N., Betton, J. M., and Alzari, P. M. (2014) Segmental helical
595 motions and dynamical asymmetry modulate histidine kinase autophosphorylation PLoS
596 Biol **12**, e1001776 10.1371/journal.pbio.1001776
- 597 41. Casino, P., Miguel-Romero, L., and Marina, A. (2014) Visualizing autophosphorylation in
598 histidine kinases Nat Commun **5**, 3258 10.1038/ncomms4258
- 599 42. Moglich, A., Ayers, R. A., and Moffat, K. (2009) Design and signaling mechanism of
600 light-regulated histidine kinases J Mol Biol **385**, 1433-1444 10.1016/j.jmb.2008.12.017

- 601 43. Lee, J., Tomchick, D. R., Brautigam, C. A., Machius, M., Kort, R., Hellingwerf, K. J. *et al.*
602 (2008) Changes at the KinA PAS-A dimerization interface influence histidine kinase
603 function *Biochemistry* **47**, 4051-4064 10.1021/bi7021156
- 604 44. Yarden, Y., and Schlessinger, J. (1987) Epidermal growth factor induces rapid,
605 reversible aggregation of the purified epidermal growth factor receptor *Biochemistry* **26**,
606 1443-1451 10.1021/bi00379a035
- 607 45. Liao, X., Liu, W., Yang, H. Q., and Jenkins, G. I. (2020) A dynamic model of UVR8
608 photoreceptor signalling in UV-B-acclimated *Arabidopsis* *New Phytol* **227**, 857-866
609 10.1111/nph.16581
- 610 46. Sang, Y., Li, Q. H., Rubio, V., Zhang, Y. C., Mao, J., Deng, X. W. *et al.* (2005) N-terminal
611 domain-mediated homodimerization is required for photoreceptor activity of *Arabidopsis*
612 CRYPTOCHROME 1 *Plant Cell* **17**, 1569-1584 10.1105/tpc.104.029645
- 613 47. Zoltowski, B. D., and Crane, B. R. (2008) Light activation of the LOV protein vivid
614 generates a rapidly exchanging dimer *Biochemistry* **47**, 7012-7019 10.1021/bi8007017
- 615 48. Zoltowski, B. D., Motta-Mena, L. B., and Gardner, K. H. (2013) Blue light-induced
616 dimerization of a bacterial LOV-HTH DNA-binding protein *Biochemistry* **52**, 6653-6661
617 10.1021/bi401040m
- 618 49. Scheuermann, T. H., Tomchick, D. R., Machius, M., Guo, Y., Bruick, R. K., and Gardner,
619 K. H. (2009) Artificial ligand binding within the HIF2alpha PAS-B domain of the HIF2
620 transcription factor *Proc Natl Acad Sci U S A* **106**, 450-455 10.1073/pnas.0808092106
- 621 50. Key, J., Hefti, M., Purcell, E. B., and Moffat, K. (2007) Structure of the redox sensor
622 domain of *Azotobacter vinelandii* NifL at atomic resolution: signaling, dimerization, and
623 mechanism *Biochemistry* **46**, 3614-3623 10.1021/bi0620407
- 624 51. Dutta, R., Qin, L., and Inouye, M. (1999) Histidine kinases: diversity of domain
625 organization *Mol Microbiol* **34**, 633-640 10.1046/j.1365-2958.1999.01646.x

- 626 52. Sievers, F., Wilm, A., Dineen, D., Gibson, T. J., Karplus, K., Li, W. *et al.* (2011) Fast,
627 scalable generation of high-quality protein multiple sequence alignments using Clustal
628 Omega Mol Syst Biol **7**, 539 10.1038/msb.2011.75
- 629 53. Letunic, I., and Bork, P. (2019) Interactive Tree Of Life (iTOL) v4: recent updates and
630 new developments Nucleic Acids Res **47**, W256-W259 10.1093/nar/gkz239
- 631 54. Sheffield, P., Garrard, S., and Derewenda, Z. (1999) Overcoming expression and
632 purification problems of RhoGDI using a family of "parallel" expression vectors Protein
633 Expr Purif **15**, 34-39 10.1006/prev.1998.1003
- 634 55. Gasteiger, E., Hoogland, C., Gattiker, A., Duvaud, S. e., Wilkins, M. R., Appel, R. D. *et*
635 *al.* (2005) Protein Identification and Analysis Tools on the ExPASy Server In The
636 Proteomics Protocols Handbook, Walker JM, ed. Humana Press, Totowa, NJ Chapter
637 Chapter 52, 571-607
- 638 56. Rueden, C. T., Schindelin, J., Hiner, M. C., DeZonia, B. E., Walter, A. E., Arena, E. T. *et*
639 *al.* (2017) ImageJ2: ImageJ for the next generation of scientific image data BMC
640 bioinformatics **18**, 529 10.1186/s12859-017-1934-z
- 641 57. Schindelin, J., Arganda-Carreras, I., Frise, E., Kaynig, V., Longair, M., Pietzsch, T. *et al.*
642 (2012) Fiji: an open-source platform for biological-image analysis Nat Methods **9**, 676-
643 682 10.1038/nmeth.2019
- 644